

# Geophysical Research Letters

## RESEARCH LETTER

10.1029/2019GL085220

### Key Points:

- Unusually high frequency EMIC waves are observed near the proton gyrofrequency with a very narrow bandwidth
- Temperature anisotropy of suprathermal protons in association with magnetosonic waves likely excites high frequency EMIC waves
- Statistical results show that high frequency EMIC waves typically occur near the equator in the low-density regions from dawn to dusk

### Correspondence to:

W. Li,  
luckymoon761@gmail.com

### Citation:

Teng, S., Li, W., Tao, X., Ma, Q., Wu, Y., Capannolo, L., et al. (2019). Generation and characteristics of unusual high frequency EMIC waves. *Geophysical Research Letters*, 46, 14,230–14,238.  
<https://doi.org/10.1029/2019GL085220>

Received 30 AUG 2019

Accepted 2 DEC 2019

Accepted article online 9 DEC 2019

Published online 20 DEC 2019

## Generation and Characteristics of Unusual High Frequency EMIC Waves

S. Teng<sup>1,2,3</sup>, W. Li<sup>3</sup>, X. Tao<sup>1,2</sup>, Q. Ma<sup>4,3</sup>, Y. Wu<sup>1,2</sup>, L. Capannolo<sup>3</sup>, X.-C. Shen<sup>3</sup>, and L. Gan<sup>3</sup>

<sup>1</sup>CAS Key Laboratory of Geospace Environment, Department of Geophysics and Planetary Sciences, University of Science and Technology of China, Hefei, China, <sup>2</sup>CAS Center for Excellence in Comparative Planetology, China, <sup>3</sup>Center for Space Physics, Boston University, Boston, MA, USA, <sup>4</sup>Department of Atmospheric and Oceanic Sciences, University of California, Los Angeles, Los Angeles, CA, USA

**Abstract** We report unusual Electromagnetic Ion Cyclotron (EMIC) waves with a very narrow frequency bandwidth, closely following and approaching the proton gyrofrequency. One interesting case analysis shows that magnetosonic waves, anisotropic suprathermal proton distributions, and high frequency EMIC waves are closely related. Magnetosonic waves potentially cause the resonant heating of suprathermal protons and the temperature anisotropy of suprathermal protons (10–100 eV) likely provides free energy for the excitation of high frequency EMIC waves. The statistical analysis shows that this type of EMIC waves has a typical wave amplitude of ~100 pT, left-handed polarization, and small wave normal angles. Moreover, these low frequency EMIC waves typically occur near the equator in the low-density regions from dawn to dusk. These newly observed high frequency EMIC waves provide new insights into understanding the generation of EMIC waves and the energy transfer between magnetosonic waves and EMIC waves.

**Plain Language Summary** Electromagnetic Ion Cyclotron (EMIC) waves are commonly observed in the Earth's magnetosphere and play an important role in causing the loss of ring current ions and relativistic electrons due to pitch angle scattering. In this study, we report unusual high frequency EMIC waves with frequency very close to the proton gyrofrequency. An interesting case study clearly shows the correlation between magnetosonic waves, the enhancement of suprathermal protons, and high frequency EMIC waves. The protons at suprathermal energies could be heated by magnetosonic waves and the anisotropic distribution of suprathermal protons is likely responsible for the excitation of high frequency EMIC waves. The statistical analysis shows that this type of EMIC waves has a typical wave amplitude of ~100 pT, left-handed polarization, and small wave normal angles. These newly observed high frequency EMIC waves provide new insights into understanding the generation of EMIC waves and the energy transfer between magnetosonic waves and EMIC waves.

## 1. Introduction

Electromagnetic ion cyclotron (EMIC) waves are intense emissions naturally occurring in the Earth's magnetosphere (Anderson et al., 1992; Mauk & McPherron, 1980; Young et al., 1981). A typical source of EMIC waves is the anisotropic distribution of energetic ions (1–100 keV) (e.g., Chen et al., 2009; Cornwall, 1965; Fraser et al., 2010; Gary et al., 1995), preferentially near the equatorial region (Loto'aniu et al., 2005). In the source region, EMIC waves are mainly left-handed polarized and propagate primarily along the magnetic field line (e.g., Min et al., 2012). During their propagation to higher latitudes, the wave vector becomes more oblique and polarization properties may change (Rauch & Roux, 1982; Thorne & Horne, 1997). The EMIC wave generation and propagation characteristics are also affected by density gradients and the abundance of heavy ions (Chen et al., 2009; Gombareff & Neira, 1983; Thorne & Horne, 1997). EMIC waves occur over various magnetic local times (MLTs) and *L*-shells (from 3 to 14), but tend to peak around the afternoon sector (Anderson et al., 1992; Min et al., 2012; Usanova et al., 2012). They often occur in three distinct bands below the gyrofrequencies of hydrogen ( $H^+$ ), helium ( $He^+$ ), and oxygen ( $O^+$ ), respectively.  $H^+$  band EMIC waves are usually found outside the plasmapause, while  $He^+$  band EMIC waves are almost equally observed inside and outside the plasmapause (e.g., Fraser & Nguyen, 2001). The excited band is controlled by the ion composition, anisotropy (Horne & Thorne, 1994), as well as the location with respect to the plasmapause (Fraser & Nguyen, 2001; Tetrick et al., 2017).

EMIC waves have received much attention due to their impact on proton and electron populations within the magnetosphere. The generated EMIC waves can result in the loss of ring current protons, thus leading

to the formation of proton aurora (Cornwall et al., 1970; Spasojevic et al., 2004; Yahnin et al., 2013). EMIC waves can also resonate with highly relativistic electrons (Engebretson et al., 2015; Sandanger et al., 2007; Thorne & Kennel, 1971) and cause pitch angle scattering loss into the atmosphere (Thorne, 1974; Thorne & Andreoli, 1980). Moreover, recent observations reported that EMIC waves can lead to subrelativistic electron precipitation. For example, Clilverd et al. (2015) showed EMIC-induced electron precipitation with a lower cutoff energy of 280 keV. Other conjunction events have also demonstrated sub-MeV electron precipitation driven by EMIC waves (e.g., Capannolo, Li, Ma, Shen, et al., 2019, Capannolo, Li, Ma, Chen, et al., 2019; Hendry et al., 2019).

One of the most important factors that determine the energy range of electrons interacting with EMIC waves is EMIC wave frequency spectra, which statistically show dependences on *L*-shell and geomagnetic activity. For H<sup>+</sup> band emissions, the average peak frequency varies between 0.25 and 0.5  $f_{cp}$ , while that of He<sup>+</sup> band emissions varies between 0.02 and 0.15  $f_{cp}$  (Meredith et al., 2014; Zhang et al., 2016), where  $f_{cp}$  is the proton gyrofrequency.

In this letter, we report an unusual EMIC wave event with a narrow frequency bandwidth at the frequency quite close to  $f_{cp}$ . A case study demonstrates a possible energy coupling process between magnetosonic waves and the observed high frequency EMIC waves. One possible generation mechanism of high frequency EMIC waves is proposed based on the calculated resonance energy and linear growth rates. Furthermore, we found 38 events with similar wave characteristics using Van Allen Probes observations and performed a statistical analysis of wave properties and preferential plasma conditions.

## 2. A Case Study of High Frequency EMIC Waves

### 2.1. Van Allen Probes Observations

The Van Allen Probes provide comprehensive plasma wave and particle measurements in the inner magnetosphere (Mauk et al., 2013). Observations of the wave magnetic field are from the Electric and Magnetic Field Instrument Suite and Integrated Science (EMFISIS; Kletzing et al., 2013). The EMFISIS suite contains the fluxgate magnetometer, the waveform frequency receiver, and the high frequency receiver. The magnetometer measures the wave frequency below 32 Hz, and waveform frequency receiver provides the wave magnetic power spectra from ~10 Hz to 12 kHz. The Helium Oxygen Proton Electron (HOPE) instrument of the Energetic Particle Composition and Thermal Plasma Suite measures electrons and ions with different species over a wide energy range from ~1 eV to ~50 keV with full pitch angle coverage (Funsten et al., 2013; Spence et al., 2013).

Figure 1 shows an overview of the Van Allen Probe A observation demonstrating interesting correlations between magnetosonic waves, suprathermal protons, and high-frequency narrow band EMIC waves. Over 16:29–17:58 UT on 1 May 2016, the spacecraft was located in the morning sector (7.7–9.1 MLT) over the *L*-shells of 4.9–5.7 near the geomagnetic equator ( $-2.5^{\circ}$ – $0.6^{\circ}$  MLAT, where MLAT represents magnetic latitude). The AE index has a value of more than 500 nT, indicating a modest substorm activity (not shown). Figure 1a shows the density profile, which is estimated from the upper hybrid resonance frequency (Kurth et al., 2015). During the time when high frequency EMIC waves were observed, the electron density slightly varied below  $15 \text{ cm}^{-3}$  (with the value of  $6 \text{ cm}^{-3}$  at ~17 UT marked by the vertical magenta line), indicating that the waves were observed outside the plasmapause. Figures 1b and 1c show the wave magnetic spectrogram and wave normal angle (WNA) in the frequency range of 10–500 Hz, with the dotted line denoting the lower hybrid resonance frequency ( $f_{LH}$ ). The values of WNA were computed onboard by the Singular Value Decomposition method (Santolik et al., 2003) and are shown only for the bins where the magnetic field wave power is larger than the background noise by at least one order of magnitude. The waves below  $f_{LH}$  have very oblique WNA nearly  $\sim 90^{\circ}$  and linear polarization (not shown), indicating the presence of magnetosonic waves. Figure 1d shows the proton flux observed by HOPE and their pitch angle distributions at the energy of 98 eV and 210 eV are shown in Figures 1e and 1f. Ring current protons with energies larger than  $\sim 10$  keV are generally the free energy source of magnetosonic waves (e.g., Ma et al., 2014). The low-energy proton population (10–200 eV) usually presents a field-aligned distribution (Yue et al., 2017), but showed peaks near  $90^{\circ}$  during this wave activity. Previous studies (Horne et al., 2000; Ma et al., 2019; Yuan et al., 2018) have shown that magnetosonic waves can cause the resonant heating of suprathermal protons in the perpendicular direction. The close correlation between the suprathermal proton enhancement

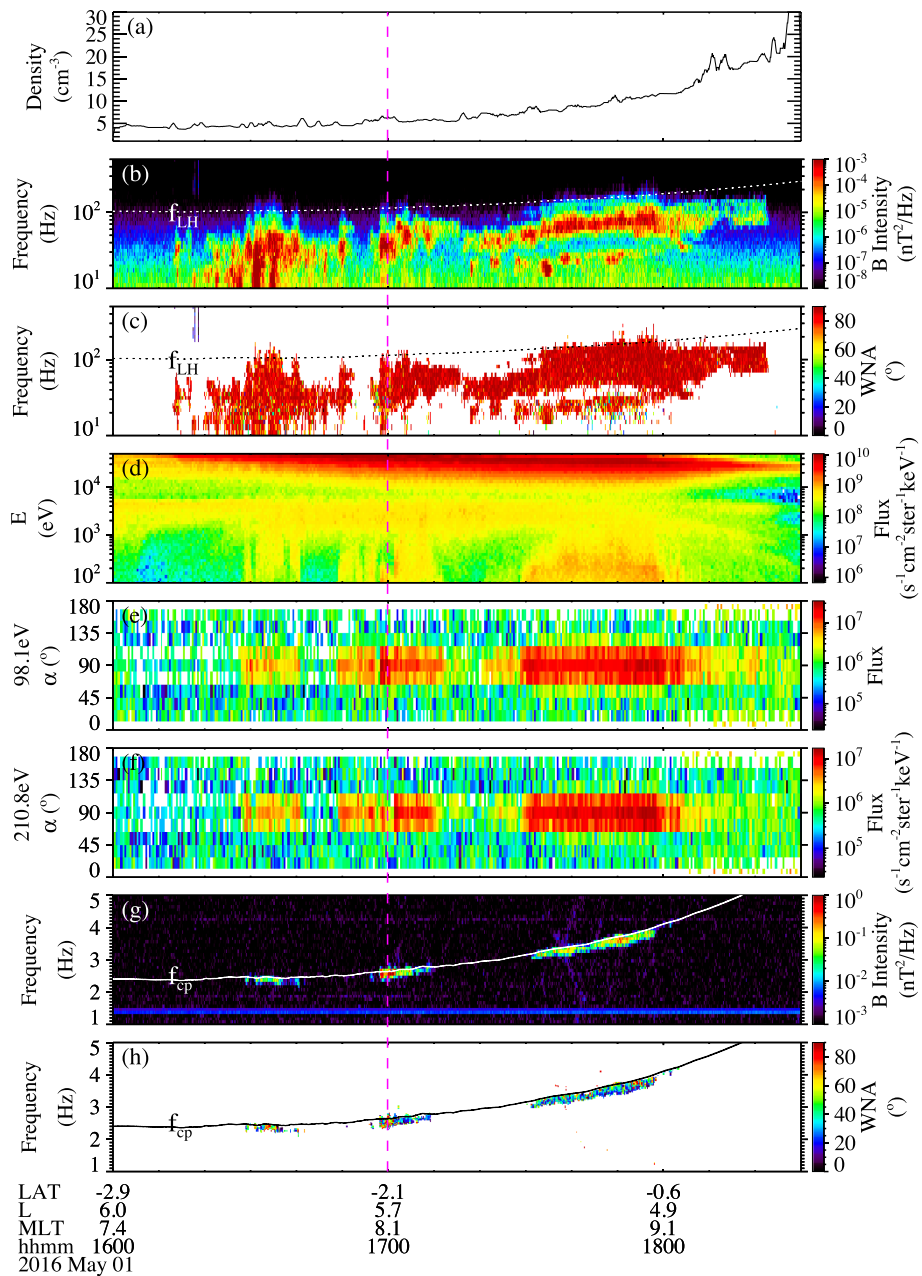


**Figure 1.** An overview of Van Allen Probe A observation on 1 May 2016. (a) The electron density profile, estimated from the identified upper hybrid frequency. (b) Magnetic power spectrogram measured by waveform frequency receiver, and (c) wave normal angle (WNA), shown in the frequency range from 10 to 500 Hz. In panels (b) and (c), the white or black dotted line represents lower hybrid resonance frequency ( $f_{LH}$ ). (d) Energy spectrogram of spin-averaged proton flux. (e and f) Pitch angle distributions of proton fluxes at energies of ~98.1 and 210.8 eV. (g) Magnetic power spectrogram measured by the magnetometer, and (h) wave normal angle shown in the frequency range from 1 to 5 Hz. The solid lines (white or black) in panels (g) and (h) represent the local proton gyrofrequency ( $f_{cp}$ ). The vertical magenta dashed line indicates the time used for the following analysis.

and the magnetosonic waves may imply the possible proton heating due to the measured magnetosonic waves.

Figure 1g displays the wave magnetic spectrogram in the frequency range between 1 and 5 Hz. Just below  $f_{cp}$ , the waves with a very narrow bandwidth are identified with the normalized peak frequency around 0.92  $f_{cp}$ , closely following and approaching  $f_{cp}$ . Figure 1h demonstrates the WNA determined using the method of

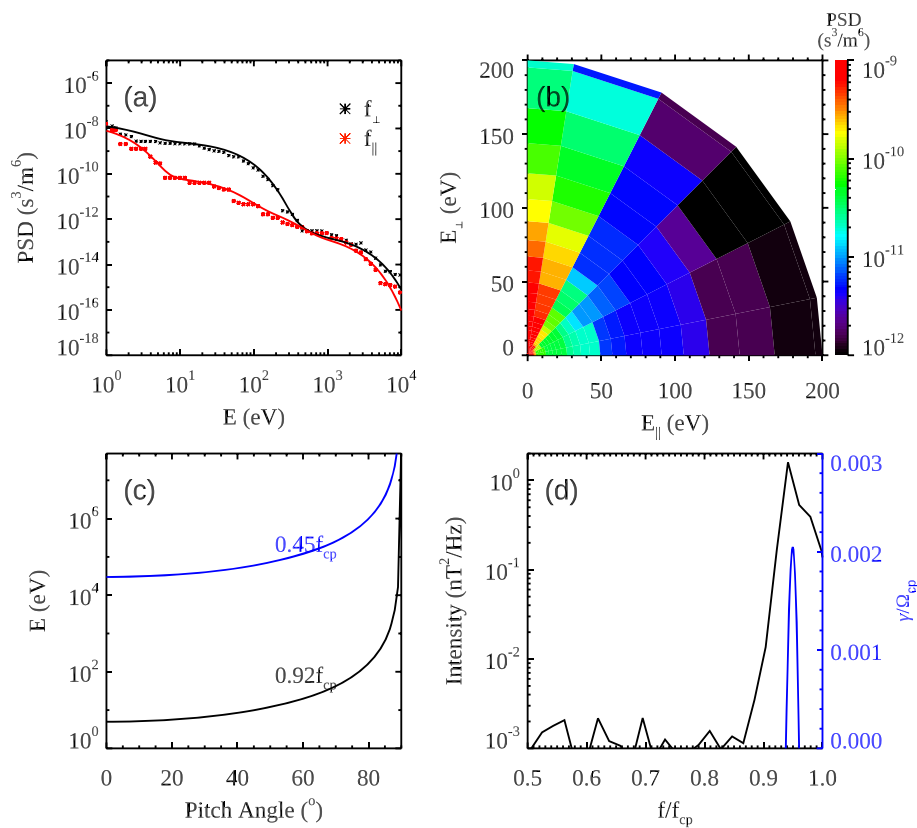


**Figure 2.** The proton distribution, proton resonance energy, and calculated EMIC wave growth rate at ~17 UT on 1 May 2016, marked by the vertical magenta line in Figure 1. (a) Parallel (red) and transverse (black) proton phase space density (PSD) measured by HOPE (dotted line) and the corresponding multicomponent fits (solid line). (b) The proton PSD distributions in the parallel and perpendicular energy space. (c) The calculated resonance energy as a function of pitch angle at the observed wave frequency  $\sim 0.92 f_{cp}$  (black) and the typical  $H^+$  band EMIC wave frequency  $\sim 0.45 f_{cp}$  (blue). (d) The comparison between the observed EMIC wave intensity (black) and the calculated linear wave growth rate (blue) using the hot plasma dispersion relation.

Means (1972). The WNAs of the observed waves were predominantly small ( $<30^\circ$ ) and the ellipticity was negative (not shown), indicating the left-handed polarization, which is consistent with the previous observations of EMIC wave properties near the source region (e.g., Min et al., 2012). Previous statistical studies of EMIC wave spectra showed that the  $H^+$  band EMIC wave power is dominant near the helium gyrofrequency (Meredith et al., 2003; Min et al., 2012; Zhang et al., 2016). The unique features of these high frequency EMIC waves, different from other common  $H^+$  band EMIC waves, are that the observed EMIC waves have a very high frequency close to  $f_{cp}$  and the frequency bandwidth is very narrow ( $\sim 0.09 f_{cp}$ ). In addition, the observed wave amplitude is around 100 pT, weaker than the typical EMIC wave amplitude of  $\sim 1$  nT, thus can be easily ignored when identifying  $H^+$  band EMIC waves.

## 2.2. Possible Generation Mechanism

To understand the excitation of such high frequency EMIC waves, we evaluate proton distribution and local plasma conditions in detail. The proton distribution from 1 eV to 50 keV measured by HOPE (Figure 1d) was used to evaluate the linear growth rate of high frequency EMIC waves based on the actual proton velocity distribution and plasma parameters. Figure 2a presents the parallel (red) and transverse (black) proton phase space densities (PSDs) and Figure 2b shows the 2-D proton PSD distribution in the energy range between 0 and 200 eV at the time indicated by the vertical magenta line in Figure 1. The pitch angle distribution of protons at suprathermal energy from a few eV to hundreds of eV exhibits a peak near  $90^\circ$  pitch angle, which is different from the statistical result showing a bidirectional field-aligned distribution for the majority of warm plasma cloak  $H^+$  (from 10 eV to several keV) (Yue et al., 2017). While EMIC waves are typically excited by an anisotropic distribution ( $T_\perp > T_\parallel$ ) of energetic ( $\sim 10\text{--}100$  keV) protons (Anderson

**Table 1**  
*Input Parameters for the BO Code to Calculate EMIC Wave Linear Growth Rates Using Hot Plasma Dispersion Relation*

	$q_s(e)$	$m_s(m/m_p)$	$n_s(\text{cm}^{-3})$	$T_{\parallel}(\text{eV})$	$T_{\perp}(\text{eV})$
#1	1	1.0	1.97	0.1	0.1
#2	1	1.0	0.444	1.06	1.75
#3	1	1.0	2.02	1.29	40.6
#4	1	1.0	0.172	28.9	28.9
#5	1	1.0	0.128	151.6	151.6
#6	1	1.0	0.235	1247	1707
#7	1	4.0	0.534	1.0	1.0
#8	1	16.0	1.0	1.0	1.0

Note. For each component,  $q_s$  represents the ratio of the species charge to the electron charge,  $m_s$  represents the ratio of the species mass to the proton mass,  $n_s$  represents the density,  $T_{\parallel}$  and  $T_{\perp}$  are parallel and perpendicular temperature.

et al., 1996; Kennel & Petschek, 1966), resonance condition suggests that the anisotropic proton distribution at lower energy might be responsible for the excitation of the observed high frequency EMIC waves.

To test whether the high frequency EMIC waves are generated by the anisotropic distribution of suprathermal (10–100 eV) protons, we calculate the resonance energy by solving the resonance condition and the cold plasma dispersion relation based on the observed wave and plasma conditions. Since the solution of the dispersion relation for a cold multi-ion plasma depends on the total ion composition, we estimate it by integrating the ion flux measured by the HOPE energy channels, which is found to be a reasonable way of calculating the actual ion composition (e.g., Blum et al., 2019). In this event, the concentration of proton, helium, and oxygen was found to be 77%, 8%, and 15%, respectively, consistent with the previous statistical result (e.g., Yue et al., 2018). Based on this ion composition, we calculate the cyclotron resonance energy of protons for the observed EMIC wave peak frequency of  $\sim 0.92 f_{cp}$  (black) and the typical  $H^+$  band EMIC wave frequency  $\sim 0.45 f_{cp}$  (blue), which are shown as a function of pitch angle in Figure 2c. Compared to the resonance energy for typical  $H^+$  band EMIC waves ( $\sim 10$  keV), the resonance energy for high frequency EMIC waves is much lower, ranging from tens to hundreds of eV. Therefore, the anisotropic proton distributions at suprathermal energy ( $\sim 10$ –100 eV), rather than ring current protons ( $\sim 10$ –100 keV), likely play a role in the excitation of high frequency EMIC waves.

Since the warm plasma effect might be important near the ion gyrofrequency (Chen et al., 2011; Silin et al., 2011), we use the BO kinetic dispersion relation solver (Xie & Yong, 2016) to calculate the linear growth rate of EMIC waves. Two-dimensional nonlinear least squares fitting is used to fit the measured proton PSD with a multicomponent nondrifting bi-Maxwellian distribution function and the fitted data in the parallel and perpendicular direction are shown in Figure 2a as the solid lines. The detailed input parameters for the BO code are listed in Table 1 and the adopted background magnetic field intensity is 173 nT. Electron, helium, and oxygen are treated as cold components and only protons contribute to the EMIC wave growth. Figure 2d shows the comparison of the calculated wave growth rate using the BO kinetic dispersion relation solver (blue) and the observed wave intensity (black). The calculated EMIC wave growth rate peaks at  $\sim 0.95 f_{cp}$  with fairly good agreement with the observations. To verify if suprathermal proton temperature anisotropy is mainly responsible for the excitation of high frequency EMIC waves, we turned off the temperature anisotropy of suprathermal protons by setting the #3 component to  $T_{\parallel} = T_{\perp} = 40.6$  eV, and found that there was no positive growth rate near  $0.95 f_{cp}$ . Therefore, the suprathermal proton temperature anisotropy is mainly responsible for the excitation of high frequency EMIC waves with little contributions from several keV protons. As discussed above, the enhanced temperature anisotropy of these suprathermal protons may result from resonant heating by magnetosonic waves. Therefore, this event suggests a possible transfer of energy from magnetosonic waves to EMIC waves through suprathermal protons.

Many previous studies investigated the correlation between EMIC and magnetosonic waves. For example, Min et al. (2016) and Min and Liu (2016) showed that a ring-like anisotropic proton velocity distribution can excite both ion Bernstein instabilities and Alfvén-cyclotron instability. Yuan et al. (2019) presented a case that EMIC waves and MS waves were simultaneously observed. The authors suggested that both waves were observed because of the modulation by the background plasma density irregularity. Yu and Yuan (2019) reported the whole evolution process of parallel EMIC waves, suggesting that it is important to

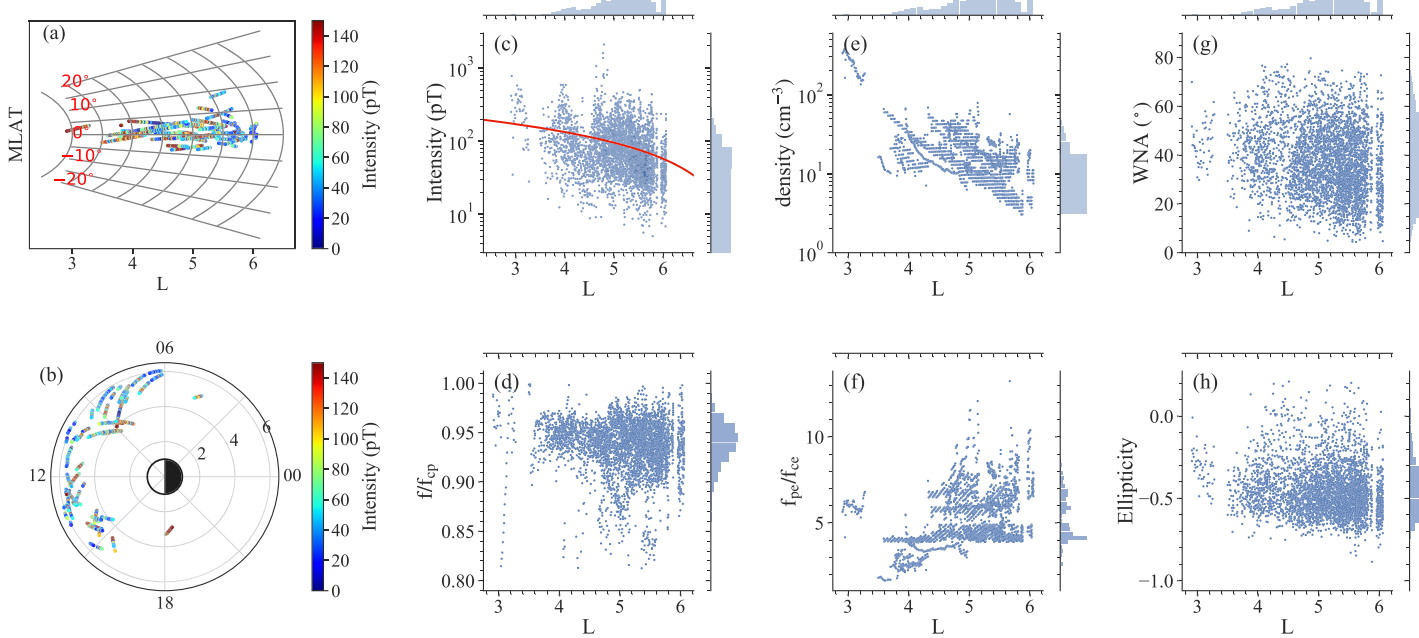


**Figure 3.** (a) The spatial distribution of high frequency EMIC wave events as a function of  $L$  versus MLAT, and (b)  $L$  versus MLT. (c) The distribution of several parameters including wave intensity, (d) peak wave frequency, (e) total electron density, (f) the ratio of electron plasma frequency to electron gyrofrequency ( $f_{pe}/f_{ce}$ ), (g) wave normal angle (WNA), and (h) ellipticity as a function of  $L$ . The marginal axis shows the distribution of the corresponding parameter as a histogram.

take into consideration the entire evolution process of wave excitation to determine the final wave amplitude. The exact energy transfer process discussed in this paper and its importance relative to previous mechanisms need further investigation and are beyond the scope of this study.

### 2.3. Minimum Resonant Energies of Electrons

EMIC waves can undergo cyclotron resonant interactions with relativistic electrons and cause pitch angle scattering loss of electrons at energies above the minimum resonance energy ( $E_{min}$ ). Previous studies suggest that  $E_{min}$  is well above 2 MeV for the majority of EMIC wave events (e.g., Jordanova et al., 2008; Meredith et al., 2003). In this case, we calculate  $E_{min}$  of the first order cyclotron resonance based on the prescribed peak wave frequency ( $0.92 f_{cp}$ ), plasma conditions, and the result of hot plasma dispersion relation solver. The obtained  $E_{min}$  is  $\sim 0.89$  MeV using equation (24) in Chen et al. (2013). This suggests that high frequency EMIC waves may play a role in driving sub-MeV electron precipitation.

## 3. Statistical Results: Characteristics of High Frequency EMIC Waves

A comprehensive survey of all high frequency EMIC waves observed by Van Allen Probes from 2012 to 2018 has been performed to identify the preferential excitation region and the statistical wave properties. The criteria for selecting these events include the following. (1) the maximum wave amplitude integrated over the frequency from  $0.75 f_{cp}$  to  $f_{cp}$  is larger than 10 pT, and (2) the field-aligned component of the wave power is less than 30% of the total magnetic wave power. After the automatic algorithm, we further filtered these events through visual inspection. The occurrence rate of such high frequency EMIC waves is relatively low and a total of 38 events were identified. The wave properties including the wave intensity, peak frequency, WNA, ellipticity, as well as other relevant parameters including the location, density, and  $f_{pe}/f_{ce}$  are recorded every 15 s, where  $f_{pe}$  and  $f_{ce}$  indicate plasma frequency and electron gyrofrequency.

The spatial distribution and statistical wave properties of EMIC waves are displayed in Figure 3. Figures 3a and 3b show the spatial distribution of these wave events on the meridian plane and equatorial plane. Mostly, these waves occur near the equator at  $|MLAT| < 5^\circ$  from dawn to dusk sector (06–16 MLT), which is overall consistent with the previous statistical results of  $H^+$  band EMIC waves (e.g., Zhang et al., 2016).

It is worth noting that the orbital coverage of Van Allen Probes was  $L < \sim 6$ , and most high frequency EMIC wave events were observed over  $L \sim 4\text{--}6$ .

Figures 3c–3h show the scatter plots of different parameters as a function of  $L$ -shell with histograms. The overplotted line in Figure 3c is the fitting result of a linear regression model, showing that the wave amplitude peaked near 100 pT, much weaker than the typically observed EMIC wave amplitudes of  $\sim 1$  nT (e.g., Zhang et al., 2016). The main reason is the very narrow frequency bandwidth, as shown in Figure 1. The wave intensity tended to decrease with increasing  $L$ -shell. It is interesting to note that for some events, which are observed at low  $L$ -shells ( $< \sim 4$ ), the wave intensity was stronger, which is probably due to the enhanced geomagnetic activities. The distribution of the peak frequency normalized to the  $f_{cp}$  is shown in Figure 3d, and the maximum probability frequency lies around  $0.95 f_{cp}$ . Although the frequency bandwidth is not shown, all these identified high frequency EMIC waves had a very narrow frequency bandwidth ( $< 0.1 f_{cp}$ ), which makes these waves different from previously observed  $H^+$  band EMIC waves. As shown in Figures 3e and 3f, most of these events were observed in the low-density region with density values below  $50 \text{ cm}^{-3}$ . The distribution of  $f_{pe}/f_{ce}$  (Figure 3f) exhibits two peaks with a major peak at  $f_{pe}/f_{ce} \sim 4$  and a secondary peak at  $f_{pe}/f_{ce} \sim 6$ . The preferential  $f_{pe}/f_{ce}$  value for the excitation of this type of waves is less than 10, consistent with the previous statistical result that EMIC wave power is dominated by the  $H^+$  band in regions of low  $f_{pe}/f_{ce}$  (e.g., Zhang et al., 2016). The wave properties including the WNA and ellipticity have been analyzed and shown in Figures 3g and 3h. The peak values of statistical WNAs and ellipticity are approximately  $30^\circ$  and approximately  $-0.5$ . The majority of high frequency EMIC waves had small-to-modest WNAs and left-handed polarization, similar to the usual EMIC wave characteristics near the source region (e.g., Saikin et al., 2015).

#### 4. Summary

In this study, we report unusual high frequency EMIC waves with frequency closely following and approaching the local  $f_{cp}$  observed by the Van Allen Probes. One event study provides a possible explanation for the excitation of these high frequency EMIC waves. In this event, which occurred on 1 May 2016, the proton distribution from 10 eV to hundreds of eV exhibited a peak near  $90^\circ$  pitch angle, different from the statistical field-aligned pitch angle distributions for warm plasma cloak  $H^+$  (e.g., Yue et al., 2017). Linear growth calculation based on the hot plasma dispersion relation indicates that a portion of suprathermal energy protons (10–100 eV) contributed to the growth of high frequency EMIC waves and the calculated growth rate agrees well with the observed wave frequency spectrum. The pancake distribution of suprathermal protons can be caused by the resonant heating due to the simultaneously observed magnetosonic waves. Further investigations of the relationship between anisotropic proton distributions at suprathermal energy and magnetosonic waves will provide a deeper understanding of the excitation of high frequency EMIC waves, but are beyond the scope of the present study.

A statistical analysis of all high frequency EMIC wave events observed by the Van Allen Probes over 2012–2018 was performed to evaluate the wave properties and preferential plasma conditions. The typical wave amplitude of high frequency EMIC waves is  $\sim 100$  pT, but some events had a stronger wave amplitude in the low  $L$ -shell region. These wave activities show the peak frequency around  $0.95 f_{cp}$  and they were mostly distributed near the equatorial region from the dawn to the dusk sector in the low-density regions with the preferential  $f_{pe}/f_{ce}$  value less than 10.

Our study is critical to improve our understanding of EMIC wave excitation and provides new insights into a potential energy transfer process between the magnetosonic and EMIC waves. The in-depth energy transfer process between magnetosonic waves, high frequency EMIC waves, and suprathermal protons is left as a future investigation and will be tested using Particle-In-Cell simulations.

#### Acknowledgments

This work was supported by NSFC grants 41631071, 41674174, and 41474142. WL, QM, LC, XS, and LG would like to acknowledge the NSF grant AGS-1723588 and the Alfred P. Sloan Research Fellowship FG-2018-10936. We thank Dr. A. V. Artemyev for the helpful discussions. We would like to thank the Van Allen Probes team for making their data available to the public and the CDAWeb for the use of AE index data. Van Allen Probes EMFISIS data were obtained from the website <https://emfisis.physics.uiowa.edu/data/index/> and data from HOPE were obtained from the website [http://www.rbsp-ect.lanl.gov/data\\_pub/](http://www.rbsp-ect.lanl.gov/data_pub/).

#### References

- Anderson, B. J., Denton, R. E., Ho, G., Hamilton, D. C., Fuselier, S. A., & Strangeway, R. J. (1996). Observational test of local proton cyclotron instability in the Earth's magnetosphere. *Journal of Geophysical Research*, 101(A10), 21,527–21,543. <https://doi.org/10.1029/96JA01251>
- Anderson, B. J., Erlandson, R. E., & Zanetti, L. J. (1992). A statistical study of Pc 1–2 magnetic pulsations in the equatorial magnetosphere: I. Equatorial occurrence distributions. *Journal of Geophysical Research*, 97, 3075–3088. <https://doi.org/10.1029/91JA02706>

- Blum, L. W., Artemyev, A., Agapitov, O., Mourenas, D., Boardsen, S., & Schiller, Q. (2019). EMIC wave-driven bounce resonance scattering of energetic electrons in the inner magnetosphere. *Journal of Geophysical Research: Space Physics*, 124, 2484–2496. <https://doi.org/10.1029/2018JA026427>
- Capannolo, L., Li, W., Ma, Q., Chen, L., Shen, X.-C., Spence, H. E., et al. (2019). Direct observation of subrelativistic electron precipitation potentially driven by EMIC waves. *Geophysical Research Letters*, 46. <https://doi.org/10.1029/2019GL084202>
- Capannolo, L., Li, W., Ma, Q., Shen, X.-C., Zhang, X.-J., Redmon, R. J., et al. (2019). Energetic electron precipitation: Multievent analysis of its spatial extent during EMIC wave activity. *Journal of Geophysical Research: Space Physics*, 124, 2466–2483. <https://doi.org/10.1029/2018JA026291>
- Chen, L., Thorne, R. M., & Bortnik, J. (2011). The controlling effect of ion temperature on EMIC wave excitation and scattering. *Geophysical Research Letters*, 38, L16109. <https://doi.org/10.1029/2011GL048653>
- Chen, L., Thorne, R. M., & Horne, R. B. (2009). Simulation of EMIC wave excitation in a model magnetosphere including structured high-density plumes. *Journal of Geophysical Research*, 114, A07221. <https://doi.org/10.1029/2009JA014204>
- Chen, L., Thorne, R. M., Shprits, Y., & Ni, B. (2013). An improved dispersion relation for parallel propagating electromagnetic waves in warm plasmas: Application to electron scattering. *Journal of Geophysical Research: Space Physics*, 118, 2185–2195. <https://doi.org/10.1002/jgra.50260>
- Clilverd, M. A., Duthie, R., Hardman, R., Hendry, A. T., Rodger, C. J., Raita, T., et al. (2015). Electron precipitation from EMIC waves: A case study from 31 May 2013. *Journal of Geophysical Research: Space Physics*, 120, 3618–3631. <https://doi.org/10.1002/2015JA021090>
- Cornwall, J. M. (1965). Cyclotron instabilities and electromagnetic emission in the ultra low frequency and very low frequency ranges. *Journal of Geophysical Research*, 70, 61–69. <https://doi.org/10.1029/JZ070i001p00061>
- Cornwall, J. M., Coroniti, F. V., & Thorne, R. M. (1970). Turbulent loss of ring current protons. *Journal of Geophysical Research*, 75, 4699. <https://doi.org/10.1029/JA075i025p04699>
- Engebretson, M. J., Posch, J. L., Wygant, J. R., Kletzing, C. A., Lessard, M. R., Huang, C. L., et al. (2015). Van Allen Probes, NOAA, GOES, and ground observations of an intense EMIC wave event extending over 12 h in magnetic local time. *Journal of Geophysical Research: Space Physics*, 120, 5465–5488. <https://doi.org/10.1002/2015JA021227>
- Fraser, B. J., Grew, R. S., Morley, S. K., Green, J. C., Singer, H. J., Loto'aniu, T. M., & Thomsen, M. F. (2010). Storm time observations of electromagnetic ion cyclotron waves at geosynchronous orbit: GOES results. *Journal of Geophysical Research*, 115, A05208. <https://doi.org/10.1029/2009JA014516>
- Fraser, B. J., & Nguyen, T. S. (2001). Is the plasmapause a preferred source region of electromagnetic ion cyclotron waves in the magnetosphere? *Journal of Atmospheric and Terrestrial Physics*, 63, 1225–1247. [https://doi.org/10.1016/S1364-6826\(00\)00225-X](https://doi.org/10.1016/S1364-6826(00)00225-X)
- Funsten, H., Skoug, R., Guthrie, A., MacDonald, E., Baldonado, J., Harper, R., et al. (2013). Helium, Oxygen, Proton, and Electron (HOPE) mass spectrometer for the radiation belt storm probes mission. *Space Science Reviews*, 179(1–4), 423–484. <https://doi.org/10.1007/s11214-013-9968-7>
- Gary, S. P., Thomsen, M. F., Yin, L., & Winske, D. (1995). Electromagnetic proton cyclotron instability: Interactions with magnetospheric protons. *Journal of Geophysical Research*, 100, 21,961–21,972. <https://doi.org/10.1029/95JA01403>
- Gomboroff, L., & Neira, R. (1983). Convective growth rate of ion cyclotron waves in a  $H^+$ - $He^+$  and  $H^+$ - $He^+$ - $O^+$  plasma. *Journal of Geophysical Research*, 88, 2170–2174.
- Hendry, A. T., Santolik, O., Kletzing, C. A., Rodger, C. J., Shiokawa, K., & Baishev, D. (2019). Multi-instrument observation of nonlinear EMIC-driven electron precipitation at sub-MeV energies. *Geophysical Research Letters*, 46, 7248–7257. <https://doi.org/10.1029/2019GL082401>
- Horne, R. B., & Thorne, R. M. (1994). Convective instabilities of electromagnetic ion cyclotron waves in the outer magnetosphere. *Journal of Geophysical Research*, 99, 17259–17273. <https://doi.org/10.1029/94JA01259>
- Horne, R. B., Wheeler, G. V., & Alleyne, H. S. C. K. (2000). Proton and electron heating by radially propagating fast magnetosonic waves. *Journal of Geophysical Research*, 105, 27,597–27,610. <https://doi.org/10.1029/2000JA000018>
- Jordanova, V. K., Albert, J., & Miyoshi, Y. (2008). Relativistic electron precipitation by EMIC waves from self-consistent global simulations. *Journal of Geophysical Research*, 113, A00A10. <https://doi.org/10.1029/2008JA013239>
- Kennel, C. F., & Petschek, H. E. (1966). Limit on stably trapped particle fluxes. *Journal of Geophysical Research*, 71(1), 1–28. <https://doi.org/10.1029/JZ071i001p00001>
- Kletzing, C., Kurth, W., Acuna, M., MacDowell, R., Torbert, R., Averkamp, T., et al. (2013). The Electric and Magnetic Field Instrument Suite and Integrated Science (EMFISIS) on RBSP. In *The Van Allen Probes Mission* (pp. 127–181). New York: Springer. <https://doi.org/10.1007/s11214-013-9993-6>
- Kurth, W. S., De Pascuale, S., Faden, J. B., Kletzing, C. A., Hospodarsky, G. B., Thaller, S., & Wygant, J. R. (2015). Electron densities inferred from plasma wave spectra obtained by the waves instrument on Van Allen Probes. *Journal of Geophysical Research: Space Physics*, 120, 904–914. <https://doi.org/10.1002/2014JA020857>
- Loto'aniu, T. M., Fraser, B. J., & Waters, C. L. (2005). Propagation of electromagnetic ion cyclotron wave energy in the magnetosphere. *Journal of Geophysical Research*, 110, A07214. <https://doi.org/10.1029/2004JA010816>
- Ma, Q., Li, W., Chen, L., Thorne, R. M., & Angelopoulos, V. (2014). Magnetosonic wave excitation by ion ring distributions in the Earth's inner magnetosphere. *Journal of Geophysical Research: Space Physics*, 119, 844–852. <https://doi.org/10.1002/2013JA019591>
- Ma, Q., Li, W., Yue, C., Thorne, R. M., Bortnik, J., Kletzing, C. A., et al. (2019). Ion heating by electromagnetic ion cyclotron waves and magnetosonic waves in the Earth's inner magnetosphere. *Geophysical Research Letters*, 46, 6258–6267. <https://doi.org/10.1029/2019GL083513>
- Mauk, B. H., Fox, N. J., Kanekal, S. G., Kessel, R. L., Sibeck, D. G., & Ukhorskiy, A. (2013). Science objectives and rationale for the Radiation Belt Storm Probes mission. *Space Science Reviews*, 179(1–4), 3–27. <https://doi.org/10.1007/s11214-012-9908-y>
- Mauk, B. H., & McPherron, R. L. (1980). An experimental test of the electromagnetic ion cyclotron instability within the Earth's magnetosphere. *Physics of Fluids*, 23(10), 2111–2127. <https://doi.org/10.1063/1.862873>
- Means, J. D. (1972). Use of the three-dimensional covariance matrix in analyzing the polarization properties of plane waves. *Journal of Geophysical Research*, 77(28), 5551–5559. <https://doi.org/10.1029/JA077i028p05551>
- Meredith, N. P., Horne, R. B., Kersten, T., Fraser, B. J., & Grew, R. S. (2014). Global morphology and spectral properties of EMIC waves derived from CRRES observations. *Journal of Geophysical Research: Space Physics*, 119, 5328–5342. <https://doi.org/10.1002/2014JA020064>
- Meredith, N. P., Thorne, R. M., Horne, R. B., Summers, D., Fraser, B. J., & Anderson, R. R. (2003). Statistical analysis of relativistic electron energies for cyclotron resonance with EMIC waves observed on CRRES. *Journal of Geophysical Research*, 108(A6), 1250. <https://doi.org/10.1029/2002JA009700>

- Min, K., Lee, J., Keika, K., & Li, W. (2012). Global distribution of EMIC waves derived from THEMIS observations. *Journal of Geophysical Research*, 117, A05219. <https://doi.org/10.1029/2012JA017515>
- Min, K., & Liu, K. (2016). Proton velocity ring-driven instabilities in the inner magnetosphere: Linear theory and particle-in-cell simulations. *Journal of Geophysical Research: Space Physics*, 121, 475–491. <https://doi.org/10.1002/2015JA022042>
- Min, K., Liu, K., & Peter Gary, S. (2016). Scalings of Alfvén-cyclotron and ion Bernstein instabilities on temperature anisotropy of a ring-like velocity distribution in the inner magnetosphere. *Journal of Geophysical Research: Space Physics*, 121, 2185–2193. <https://doi.org/10.1002/2015JA022134>
- Rauch, J. L., & Roux, A. (1982). Ray tracing of ULF waves in a multicomponent magnetospheric plasma: Consequences for the generation mechanism of ion cyclotron waves. *Journal of Geophysical Research*, 87(10), 8191–8198. <https://doi.org/10.1029/JA087iA10p08191>
- Saikin, A. A., Zhang, J.-C., Allen, R. C., Smith, C. W., Kistler, L. M., Spence, H. E., et al. (2015). The occurrence and wave properties of H<sup>+</sup>, He<sup>+</sup>, and O<sup>+</sup>-band EMIC waves observed by the Van Allen Probes. *Journal of Geophysical Research: Space Physics*, 120, 7477–7492. <https://doi.org/10.1002/2015JA021358>
- Sandanger, M., Søraas, F., Aarsnes, K., Oksavik, K., & Evans, D. S. (2007). Loss of relativistic electrons: Evidence for pitch angle scattering by electromagnetic ion cyclotron waves excited by unstable ring current protons. *Journal of Geophysical Research*, 112, A12213. <https://doi.org/10.1029/2006JA012138>
- Santolik, O., Parrot, M., & Lefèuvre, F. (2003). Singular value decomposition methods for wave propagation analysis. *Radio Science*, 38(1), 1010. <https://doi.org/10.1029/2000RS002523>
- Silin, I., Mann, I. R., Sydora, R. D., Summers, D., & Mace, R. L. (2011). Warm plasma effects on electromagnetic ion cyclotron wave MeV electron interactions in the magnetosphere. *Journal of Geophysical Research*, 116, A05215. <https://doi.org/10.1029/2010JA016398>
- Spasojevic, M., Frey, H. U., Thomsen, M. F., Fuselier, S. A., Gary, S. P., Sandel, B. R., & Inan, U. S. (2004). The link between a detached subauroral proton arc and a plasmaspheric plume. *Geophysical Research Letters*, 31, L04803. <https://doi.org/10.1029/2003GL018389>
- Spence, H. E., Reeves, G. D., Baker, D. N., Blake, J. B., Bolton, M., Bourdarie, S., et al. (2013). Science goals and overview of the Radiation Belt Storm Probes (RBSP) Energetic Particle, Composition, and Thermal Plasma (ECT) suite on NASA's Van Allen Probes mission. *Space Science Reviews*, 179(1–4), 311–336. <https://doi.org/10.1007/s11214-013-0007-5>
- Tetrick, S. S., Engebretson, M. J., Posch, J. L., Olson, C. N., Smith, C. W., Denton, R. E., et al. (2017). Location of intense electromagnetic ion cyclotron (EMIC) wave events relative to the plasmapause: Van Allen Probes observations. *Journal of Geophysical Research: Space Physics*, 122, 4064–4088. <https://doi.org/10.1002/2016JA023392>
- Thorne, R. M. (1974). A possible cause of dayside relativistic electron precipitation events. *Journal of Atmospheric and Terrestrial Physics*, 36, 635–645.
- Thorne, R. M., & Andreoli, L. J. (1980). Mechanisms for intense relativistic electron precipitation, in *Exploration of the Polar Upper Atmosphere*. In C. S. Deehr & J. A. Holtet (Eds.), (p. 381). Hingham, Mass: D. Reidel Pub. Co.
- Thorne, R. M., & Horne, R. B. (1997). Modulation of electromagnetic ion cyclotron instability due to interaction with ring current O<sup>+</sup> during magnetic storms. *Journal of Geophysical Research*, 102(96), 14155–14163. <https://doi.org/10.1029/96JA04019>
- Thorne, R. M., & Kennel, C. F. (1971). Relativistic electron precipitation during magnetic storm main phase. *Journal of Geophysical Research*, 76, 4446–4453. <https://doi.org/10.1029/JA076i019p04446>
- Usanova, M. E., Mann, I. R., Bortnik, J., Shao, L., & Angelopoulos, V. (2012). THEMIS observations of electromagnetic ion cyclotron wave occurrence: Dependence on AE, SYMH, and solar wind dynamic pressure. *Journal of Geophysical Research*, 117, A10218. <https://doi.org/10.1029/2012JA018049>
- Xie, H., & Yong, X. (2016). PDRK: A general kinetic dispersion relation solver for magnetized plasma. *Plasma Science and Technology*, 18(2), 97–107. <https://doi.org/10.1088/1009-0630/18/2/01>
- Yahnin, A. G., Yahnina, T. A., Frey, H., & Pierrard, V. (2013). Sub-oval proton aurora spots: Mapping relatively to the plasmapause. *Journal of Atmospheric and Solar - Terrestrial Physics*, 99, 61–66. <https://doi.org/10.1016/j.jastp.2012.09.018>
- Young, D. T., Perraut, S., Roux, A., deVilledary, C., Gendrin, R., Korth, A., et al. (1981). Wave-particle interactions near  $\Omega_{He+}$  observed on GEOS 1 and 2.1. Propagation of ion cyclotron waves in He<sup>+</sup>-rich plasma. *Journal of Geophysical Research*, 86(A8), 6755–6772. <https://doi.org/10.1029/JA086iA08p06755>
- Yu, X., & Yuan, Z. (2019). Saturation characteristics of parallel EMIC waves in the inner magnetosphere. *Geophysical Research Letters*, 46, 7902–7910. <https://doi.org/10.1029/2019GL083630>
- Yuan, Z., Yu, X., Huang, S., Qiao, Z., Yao, F., & Funsten, H. O. (2018). Cold ion heating by magnetosonic waves in a density cavity of the plasmasphere. *Journal of Geophysical Research: Space Physics*, 123, 1242–1250. <https://doi.org/10.1002/2017JA024919>
- Yuan, Z., Yu, X., Ouyang, Z., Yao, F., Huang, S., & Funsten, H. O. (2019). Simultaneous trapping of electromagnetic ion cyclotron and magnetosonic waves by background plasmas. *Journal of Geophysical Research: Space Physics*, 124, 1635–1643. <https://doi.org/10.1029/2018JA026149>
- Yue, C., Bortnik, J., Li, W., Ma, Q., Gkioulidou, M., Reeves, G. D., et al. (2018). The composition of plasma inside geostationary orbit based on Van Allen Probes observations. *Journal of Geophysical Research: Space Physics*, 123, 6478–6493. <https://doi.org/10.1029/2018JA025344>
- Yue, C., Bortnik, J., Thorne, R. M., Ma, Q., An, X., Chappell, C. R., et al. (2017). The characteristic pitch angle distributions of 1 eV to 600 keV protons near the equator based on Van Allen Probes observations. *Journal of Geophysical Research: Space Physics*, 122, 9464–9473. <https://doi.org/10.1002/2017JA024421>
- Zhang, X.-J., Li, W., Thorne, R. M., Angelopoulos, V., Bortnik, J., Kletzing, C. A., et al. (2016). Statistical distribution of EMIC wave spectra: Observations from Van Allen Probes. *Geophysical Research Letters*, 43, 12,348–12,355. <https://doi.org/10.1002/2016GL071158>